Published in final edited form as:
Microb Pathog. 2013 February ; 55: 39–50. doi:10.1016/j.micpath.2012.09.011.

A non-invasive *in vivo* imaging system to study dissemination of bioluminescent *Yersinia pestis* CO92 in a mouse model of pneumonic plague

Jian Sha[1,±], **Jason A. Rosenzweig**[2,±], **Michelle L. Kirtley**[1], **Christina J. van Lier**[1], **Eric C. Fitts**[1], **Elena V. Kozlova**[1], **Tatiana E. Erova**[1], **Bethany L. Tiner**[1], and **Ashok K. Chopra**[1,3,4,5,*]

[1]Department of Microbiology & Immunology, University of Texas Medical Branch, Galveston, Texas, USA

[2]Department of Biology, Center for Bionanotechnology and Environmental Research (CBER), Texas Southern University, Houston, Texas, USA

[3]Sealy Center for Vaccine Development, University of Texas Medical Branch, Galveston, Texas, USA

[4]Institute of Human Infections & Immunity, University of Texas Medical Branch, Galveston, Texas, USA

[5]Galveston National Laboratory, University of Texas Medical Branch, Galveston, Texas, USA

Abstract

The gold standard in microbiology for monitoring bacterial dissemination in infected animals has always been viable plate counts. This method, despite being quantitative, requires sacrificing the infected animals. Recently, however, an alternative method of *in vivo* imaging of bioluminescent bacteria (IVIBB) for monitoring microbial dissemination within the host has been employed. *Yersina pestis* is a Gram-negative bacterium capable of causing bubonic, septicemic, and pneumonic plague. In this study, we compared the conventional counting of bacterial colony forming units (cfu) in the various infected tissues to IVIBB in monitoring *Y. pestis* dissemination in a mouse model of pneumonic plague. By using a transposon mutagenesis system harboring the luciferase (*luc*) gene, we screened approximately 4000 clones and obtained a fully virulent, *luc*-positive *Y. pestis* CO92 (*Y. pestis*-*luc2*) reporter strain in which transposition occurred within the largest pMT1 plasmid which possesses murine toxin and capsular antigen encoding genes. The aforementioned reporter strain and the wild-type CO92 exhibited similar growth curves, formed capsule based on immunofluorescence microscopy and flow cytometry, and had a similar LD_{50}. Intranasal infection of mice with 15 LD_{50} of CO92-*luc2* resulted in animal mortality by 72 h, and an increasing number of bioluminescent bacteria were observed in various mouse organs over a 24–72 h period when whole animals were imaged. However, following levofloxacin treatment (10 mg/kg/day) for 6 days 24 h post infection, no luminescence was observed after 72 h of infection, indicating that the tested antimicrobial killed bacteria preventing their detection in host peripheral tissues. Overall, we demonstrated that IVIBB is an effective and non-invasive way of monitoring

*Address for correspondence: A.K. Chopra Department of Microbiology & Immunology, 301 University Blvd., UTMB, Galveston, TX 77555-1070, USA achopra@utmb.edu; Telephone: 409-747-0578; Fax 409-747-6869.
±Both authors contributed equally

bacterial dissemination in animals following pneumonic plague having strong correlation with cfu, and our reporter CO92-*luc2* strain can be employed as a useful tool to monitor the efficacy of antimicrobial countermeasures in real time.

Keywords

Bioluminescent *Y. pestis*; pneumonic plague; *in vivo* imaging; levofloxacin; immunofluorescence microscopy; flow cytometry; bacterial dissemination

1. Introduction

Yersinia pestis, one of three human pathogenic yersiniae species, has a complicated life cycle occurring in both arthropod vectors and mammalian hosts (e.g. rats, squirrels, and prairie dogs). Unfortunately, the arthropod vector can transmit the pathogen to humans in close proximity to animal reservoirs [1]. The notorious pathogen is responsible for over 200 million deaths stemming from the three major human plague pandemics that it has caused [2, 3]. In sharp contrast, the closely related pathogenic yersiniae, *Y. pseudotuberculosis* and *Y. enterocolitica* cause a relatively benign self-limiting gastro-intestinal disease in humans [4]. Today, plague continues to be a problem in endemic regions of India and China where rodent populations tend to be high. In fact, there are approximately 1000–2000 human infection cases globally with some instances of infection occurring in the four corners region of the United States (where Arizona, Colorado, New Mexico, and Utah meet) as well as in parts of California [5, 6].

Presently, the World Health Organization has designated plague caused by *Y. pestis* as a re-emerging infectious disease [7, 8]. More importantly, the weaponization of a multiple-drug resistant *Y. pestis* strain poses a significant health threat to society [9, 10]. Since several clinical isolates of *Y. pestis* have naturally acquired resistance to chloramphenicol, streptomycin, and penicillin derivatives [11, 12], recent studies have evaluated the efficacy of new classes of antimicrobials including the fluoroquinolone levofloxacin and a ketolide cethromycin in animal models of plague [13, 14]. Even though both of the aforementioned drugs cleared the plague bacilli when treatment was initiated within 48 h of infection in a rat model of pneumonic plague [14], additional novel anti-plague drugs need to be developed, evaluated, and made available to the public. Only recently, levofloxacin was approved by the Food and Drug Administration (FDA) for plague, and this approval was based solely on animal efficacy data (http://www.fda.gov/NewsEvents/Newsroom/PressAnnouncements/ucm302220.htm). Furthermore, many plague researchers are also alternatively working to develop an efficacious plague vaccine since currently no vaccine is available for human use [15].

Taking into consideration the threat of multiple-drug resistant *Y. pestis* in a biological warfare setting, against which we have no effective prophylactic vaccine or antimicrobials, a reporter strain that can provide real-time dissemination information within a host could be a useful tool when testing the efficacy of novel chemotherapeutics. Similarly, such a tool would prove useful when holistically measuring the virulence potential of a live-attenuated vaccine candidate strain or to demonstrate protective efficacy of a subunit vaccine against plague. In fact, bioluminescent imaging (BLI) has been used for monitoring the dissemination of *Burkholderia* following a respiratory infection in mice [16]. While our studies were in progress, Nham et al. reported monitoring dissemination of *Y. pestis* in BALB/c mice in a bubonic plague model of infection [17]. In both instances, BLI allowed for real-time, semi-quantitative visualization of bacterial loads in various tissues following bacterial dissemination from the sites of infection at multiple time points. BLI takes

advantage of either ectopic, plasmid-driven or transposon-mediated, chromosomally-integrated expression of a luciferase (*luc*) gene [16].

In this study, we employed the transposon-encoded luminescence operon (pUTmini-Tn*5::lux*Km2) to generate our *Y. pestis* reporter strain, *Y. pestis-luc2*. The reporter strain did not suffer any attenuation in its virulence potential, and the *luc* gene was stably expressed following its insertion into the pMT1 plasmid. We then characterized bacterial dissemination of *Y. pestis-luc2* in Swiss-Webster mice at various time-points and determined the impact of levofloxacin treatment (24-h post infection) on bacterial dissemination using IVIBB.

2. Results

2.1 Generation and characterization of the Y. pestis-luciferase (luc) reporter strains

Since IVIBB has not been previously employed to monitor dissemination of *Y. pestis* CO92 following an intranasal challenge of mice, we sought to characterize the utility of such an approach in evaluating the efficacy of an antimicrobial treatment in preventing bacterial dissemination. Therefore, *Y. pestis* CO92 cells were transformed with pUTmini-Tn*5::lux*Km2 plasmid. We screened approximately 4,000 colonies, indicating either insertion of the transposon into bacterial chromosome or plasmids or the possibility of transposon-harboring free plasmid in *Y. pestis*. Upon, *in vivo* image analysis of these clones, 5 colonies were initially bioluminescent, and 2 of them (*luc1* and *luc2*) exhibited strong bioluminescence with radiance above 5×10^6 ρ/sec (i.e., total flux). These 2 clones were then used to intranasally challenge mice with a 15 LD_{50}. One clone (*luc2*) consistently exhibited better bioluminescence in animals compared to the other clone (*luc1*; data not shown).

We then examined these two clones to determine the site of transposon insertion. Within *luc2*, the transposon insertion was at 1020 base pairs (bp) downstream of the murine toxin gene (*ymt*) start codon (located within the pMT1 plasmid). Within *luc1,* the transposon insertion was 603 bp downstream of the long-chain fatty acid outer membrane transporter gene (*fadL*) start codon. The encoded FadL is essential for the uptake of long-chain fatty acids (C12 to C18) in *Escherichia coli* [18].

To ensure that the insertion of transposon harboring the *luc* gene did not disrupt the *caf1* (encoding capsular antigen F1, a virulence associated factor) open reading frame, we used anti-F1 primary antibodies followed by secondary antibodies conjugated to Alexa Fluor 488 or 594 prior to performing flow cytomteric/immunofluorescence analyses. Doing so enabled us to evaluate the presence of F1 antigen in both the *Y. pesitis-luc2* reporter and its parental CO92 strain. Relative to the isogenic parental strain, the reporter *Y. pestis-luc2* exhibited a very similar emission spectrum by fluorescent activated cell sorting (FACS) analysis, demonstrating that the *caf1* open reading frame was not disrupted by the integration of the *luc* gene into the pMT1 plasmid (Fig. 1A). The one advantage to employing FACS is that it allows for the analysis of individual cells; as a result, we have used FACS previously for that very reason [19, 20]. In addition, we also examined the presence of F1 antigen on bacterial surface by performing immunofluorescence microscopy. The wild-type (WT) *Y. pestis* CO92 and its two *luc* reporter strains (*luc1 and luc2*) exhibited the presence of F1 antigen (Fig. 1B). As expected, the isogenic Δ*caf1* mutant of CO92 strain was devoid of the F1 antigen (Fig. 1B).

To ensure that growth rates were similar between the WT and *luc2* reporter strain, colony forming units (cfu) were enumerated after liquid culture samples were removed every 2 h for a 12 h period revealing essentially no difference between the two strains' growth rates

(Fig. 2A). To characterize the *Y. pestis-luc2* reporter strain using a pneumonic plague infection model system, mice were intranasally challenged with 5 LD_{50} of either the *Y. pestis-luc2* reporter strain or the isogenic WT strain. The 80% lethality induced by *Y. pestis-luc2* (achieved 5 days post- infection) mirrored that of its parental strain (Fig. 2B). Taken together, insertion of the reporter gene in the *Y. pestis luc2* strain did not affect its growth or virulence potential. The use of 5 LD_{50} allowed us to better discern any difference in virulence between the WT CO92 and its *luc2* reporter strain.

2.2 IVIBB and correlation with Y. pestis dissemination in mice

After determining that *Y. pestis-luc2* was fully virulent and did not demonstrate a compromised growth rate, we infected mice (n=9) intranasally with 15 LD_{50} and measured bioluminescence at 24, 36, 48, 60 and 72 h post-infection to evaluate progression of infection in the same animals (Fig. 3). In addition, another 15 mice were infected with 15 LD_{50} of *Y. pestis-luc2*, and at 24, 48, and 72 h post infection, we determined cfu in lungs, liver, spleen, and blood of 5 animals per time point. At 24 and 36 h post-infection, essentially no bioluminescence was observed in whole anesthetized animals (Figs. 3A&B and 4A), and no dissemination of bacteria was noted in liver, spleen, or blood via the viable plate count method (after 24 h) when homogenized tissues or blood was used (Fig. 4A). Only lungs were positive for *Y. pestis-luc2* and 4/5 mice had cfu in the range of 1.4×10^3–4.3×10^5/organ, with one animal having cfu of 5.0×10^2. The radiance values of all the animals remained within a log of the control animal values after both 24 and 36 h for all the selected organs (Fig. 3F).

At 48 and 60 h post-infection, *Y. pestis-luc2* disseminated to other organs in mice (Fig. 3C&D) and bioluminescence was observed in whole anesthetized animals in anatomical regions of interest (ROIs) where lungs, liver, and spleen would be located (e.g., mouse #s 148 and 152). The total flux values observed at 48 and 60 h post-infection were highest in those animals with the greatest observable radiance in the images; likewise, profuse dissemination of bioluminescence bacteria was noted in those same mice (e.g., mouse #s 151 and 154) at the 60 h post-infection time-point (Fig. 3D&F). Bacterial dissemination was also apparent from viable plate counts at 48 h post-infection of homogenized lungs (average of 9.4×10^6 cfu/organ), homogenized liver (average of 5.4×10^5 cfu/organ), homogenized spleen (average of 4.4×10^5 cfu/organ), or blood (average of 6.1×10^4 cfu/ml) (Fig. 4B).

By 72 h following infection, there was dramatic bacterial dissemination as measured by both IVIBB (Figs. 3E&F and 4C) and viable plate counts of infected tissues (Fig. 4C). IVIBB demonstrated a profuse dissemination wherein *Y. pestis-luc2* could be found virtually throughout the entire animals' bodies (3/5 mice; mouse #s 153, 166, and 170 [Fig. 4C]), with the most intense bioluminescence in regions corresponding to the lungs, liver, and spleen (Fig. 4C). It is of interest to note that bioluminescence decreased in mice at 72 h post infection that were found dead at the time of imaging (Fig. 3E&F; mouse #s 146, 147, and 155).

Bacterial loads at 72 h post-infection in the lungs were (average 6.8×10^8) cfu/organ, in the liver were (average of ~2.0×10^9) cfu/organ, in the spleen were (average of ~1.5×10^9) cfu/organ, and in the blood were (average of ~1.7×10^9) cfu/ml (Fig. 4C). A peak total flux of ~10^7 ρ/sec, ~10^8 ρ/sec, and ~10^7 ρ/sec was obtained for lungs, liver, and spleen, respectively which represented an increase of between 3–4 logs from the control animals between timeframe of 24–60 h post-infection. (Figs. 3F and 4D) In fact, there was a strong correlation between bioluminescence (radiance) and bacterial loads (as determined by viable plate counts) in each organ/tissue analyzed between 24–72 h time-point. This was evidenced by R (regression) values of 0.91, 0.96, 0.99, and 0.99 corresponding to lung cfu vs. radiance,

spleen cfu vs. radiance, liver cfu vs. radiance, and blood cfu vs. radiance, respectively (Fig. 4E).

2.2 IVIBB and correlation with colony forming units in excised organs

To better acquire IVIBB in infected tissues, harvested organs themselves were scanned rather than imaging the whole animals. Doing so allowed for a direct comparison of bioluminescence intensity in 5 infected animals' tissues and bacterial loads via viable plate counts at 24 (Fig. 5A), 48 (Fig. 5B), and 72 (Fig. 5C) h post-infection. By 24 h post-infection, bacterial loads were less than 1.0×10^5 in most cases which did not produce any detectable radiance and measured radiances were less than 10^5 ρ/sec (Fig. 5A&D). By 48 h post infection, bioluminescence was detected visually in the lung tissues of 4/5 infected animals although an average radiance value 8.7×10^5 ρ/sec was observed in all of the 5 mice, which corresponded to bacterial loads of an average of 9.4×10^6 cfu (Fig. 5B&D). At 72 h post infection, there was strong bioluminescence of at least 3.2 x10^6 ρ/sec in lungs, liver, and spleen corresponding to cfu counts of $4.0–4.5 \times 10^7$ in lungs and spleen (Fig. 5C&D). In fact, viable cfu in each of the aforementioned tissues and bioluminescence over 24–72 h post infection exhibited a strong correlation in all tissues evaluated (Fig. 5E). More specifically, R values were 0.96, 0.99, and 0.99 for lung cfu vs. radiance, spleen cfu vs. radiance, and liver cfu vs. radiance respectively. Thus, in both excised organs as well as in organs from whole bodies of mice, imaging followed by quantification of radiance using ROIs demonstrated significant correlation with cfu in lungs, liver, spleen, and or blood.

Finally, bioluminescence of *Y. pestis-luc2* bacterial colonies, recovered from lung tissues, was acquired. The rationale for this study was to confirm that the organisms isolated from the lung tissue homogenates were the same as the initial culture used for infection of mice and to determine stability of the reporter strain to produce bioluminescence. A representing plate with varying dilutions of the lung homogenates is shown in Fig. 6, and the colonies exhibited radiance values of 2.8×10^8 ρ/sec.

2.4 IVIBB demonstrates reduced microbial dissemination in mice following levofloxacin treatment

We then evaluated whether IVIBB could be an appropriate tool for measuring the efficacy of administered antimicrobials following intranasal challenge of mice with 15 LD_{50} of *Y. pestis-luc2*. For these experiments, we employed the fluoroquinolone levofloxacin, which we had used in pneumonic models of plague previously [13, 14]. Levofloxacin was administered intraperitoneally (i.p.) at a dose of 10 mg/kg/day for 6 days 24 h post challenge. At 72 h post-infection, IVIBB was acquired, and bacterial loads in lungs, liver, spleen, and blood were determined by viable plate counting. The 72 h time point was chosen for the levofloxacin studies since at this time point the greatest degree of dissemination of bacteria occurred within animals when no antimicrobials were given (Fig. 4C). Interestingly, bioluminescence levels were comparable to those observed in non-infected control animals when levofloxacin was administered 24 h post infection (Figs. 7 and 3F). As determined by viable plate counts, there were no bacterial loads in liver, spleen, or blood (Fig. 7). This strongly suggested that the reason why there was no observed bioluminescence in levofloxacin treated mice was due to lack of bacterial dissemination on account of the bactericidal activity of levofloxacin-mediated inhibition of DNA gyrase. Even in the lung tissue itself of levofloxacin treated mice, the site of infection during the intranasal challenge, only an average of 1.8×10^4 cfu/organ were observed (Fig. 7) compared to an average of 6.8×10^8 cfu/organ load in lung tissue derived from untreated (no levofloxacin) mice at 72 h post infection (Fig. 4C). In fact, by day 7 post infection in levofloxacin treated mice, there were no detectable cfu in lung tissues (Fig. 7 inset). For these studies, we preferred to use 15 LD_{50} of *Y. pestis-luc2* so that we could better discern antimicrobial nature of levofloaxcin.

As carried out for non-levofloxacin treated mice, tissues were harvested from levofloxacin-treated mice to determine bioluminescence of organs alone, rather than holistically scanning the entire animal (Fig. 8). As was expected, bioluminescence was at levels of non-infected mice for liver and spleen but a slight increase in lung bioluminescence over non-infected animal levels was noted when total flux was measured, with no apparent bioluminescence in the images for any of the organs. In fact, it appeared that when bacterial loads drop below 10^5 cfu, bioluminescence could no longer be detected by eye against background radiance in the images (Fig. 8).

3. Discussion

Y. pestis is a formidable pathogen against which we currently have no effective vaccine [15]. The imposing threat of a bio-attack against civilians by a weaponized multiple-drug resistant *Y. pestis* strain (that is either naturally occurring or has been engineered) has prompted the evaluation of several antimicrobial agents in rat and murine models of infection [13, 14]. In fact, levofloxacin which is effective in rodent and non-human primate models of pneumonic plague was recently approved by FDA for human use [13, 14, 21]. However, additional chemotherapeutics are still needed and being developed, and a facile, real-time reporter strain, like *Y. pestis-luc2*, can provide researchers a way in which to quickly measure antimicrobial efficacy in animal models of infection. In this manuscript, we demonstrated that IVIBB is an effective tool for measuring bacterial dissemination in a pneumonic plague infection model using outbred Swiss-Webster mice.

Bioluminescence has been reported to accurately measure bacterial dissemination of both *Burkholderia* and *Y. pestis* in BALB/c mice in recent reports [16, 17]. However, unlike our studies, the recently published bioluminescence study of *Y. pestis* followed a mouse model of bubonic plague [17]. We believe that a pneumonic model of infection more accurately represents how the pathogen would be spread following an above mentioned bio-attack. Our recent studies demonstrated that mice and rats infected with *Y. pestis* via either intranasal or aerosol route exhibited similar kinetics of disease progression, bacterial dissemination, organs' histopathology and cytokine production [22, 23]. By using bioluminescence reporter strain, we have viewed dissemination of *Y. pestis* for the first time in real time following intranasal challenge. There seems to be animal-to-animal variation in the kinetics of dissemination of bacteria. For example, the infection seemed to be confined to one lung (mice #146, 147, 150, and 153), while in other mice (#148, 151, 152, 154, and 160), the organism disseminated widely to peripheral organs. However, irrespective of this variation in bacterial spread from one animal to another, the infection was invariably been fatal (Fig. 3).

The insertion of the luciferase reporter gene occurred in the *ymt* gene, encoding the murine toxin, allowing for the toxin promoter to drive expression of the genes encoding luciferase enzyme and the substrate. Murine toxin is homologous to the phosplipase D superfamily of proteins and is essential for successful transmission of bacteria from a flea vector [24, 25]. Disruption of the *ymt* gene has been shown to negligibly affect the virulence of *Y. pestis* mutant strains [24].

Our data strongly support previously published reports that claim bioluminescence imaging is an effective real-time method to monitor bacterial dissemination of *Salmonella* Typhymurium [26], *E. coli* [27], *Mycobacterium tuberculosis* [28], *Burkholderia* [16], *Y. pestis* during bubonic plague [17], and now pneumonic plague (this study). Generally, the intensity of luminescence correlated well with bacterial loads (Fig. 4D and 5D.), although it might still be affected by other factors such as the expression level of the luminescence gene, type of tissues examined, and the condition of the examined tissues. Despite the

possible lack of correlation between radiance and cfu loads at the level of organs in dead animals (Fig 3E) potentially due to diminished oxygenation in deceased animals, both whole mouse imaging of live mice as well as imaging of excised organs clearly showed a significant correlation of luminescence intensity with cfu from lung, liver, spleen, and blood. Taken together, these data demonstrated that IVIBB is an effective way to measure bacterial dissemination of *Y. pestis* following an intranasal challenge in real time, albeit in a slightly less sensitive manner than viable plate counts. Further, IVIBB can be extremely useful in measuring the efficacy of novel antimicrobial agents in killing and preventing bacterial dissemination. Additionally, IVIBB can also be useful for measuring the virulence potential of putative live-attenuated vaccine candidate strains in real time.

4. Materials & Methods

4.1 Strains and reagents

For all mouse infections, the fully virulent *Y. pestis* CO92 strain (obtained from the Biodefense and Emerging Infections [BEI] Research Resources Repository, Manassas, VA) was used. The out-bred Swiss-Webster mice were purchased from Taconic, Germantown, NY.

The *Y. pestis*-luciferase (*luc*) reporter strains were generated following electroporation of pUTmini-Tn*5::lux*Km2 plasmid as previously described [16] into the *Y. pestis* CO92 strain. This mini-transposon contains a promoterless luminescence operon *lux* and a kanamycin cassette for transposon selection [29]. The *lux* operon consists of five genes, *luxCDABE*. The *luxCDE* operon encodes a fatty acid reductase complex involved in synthesis of the fatty aldehyde substrate for the luminescence reaction catalyzed by the luciferase LuxAB subunits [30]. Only those transposon mutant strains in which the *lux* operon is under the control of an active gene promoter from the *Y. pestis* genome will produce luminescence [17]. Following the screening of transposon mutants, the colonies stably expressing and producing the greatest amount of luminescence were selected for all subsequent studies. The insertion sites of transposons in two such mutant colonies that optimally produced luciferase were determined by chromosomal walking by using primer T7: 5′GCACTTGTGTATAAGAGTCAG 3′ which corresponds to the DNA sequence adjacent to the O-end of mini-transposon Tn*5* [31].

4.2 Growth curves and fluorescent activated cell sorting [FACS])/immunoflourescence

The WT *Y. pestis* CO92 and its *luc2* mutant were grown to saturation and subsequently diluted 1:100 with 50 ml of Heart infusion broth (HIB) medium into a HEPA-filtered TOP polycarbonate Erlenmeyer culture flasks (OD ~ 0.1). Subcultures were grown at 28°C with agitation for 12 h. Samples from each flask were taken at 2 h intervals, and serial dilutions were used for viable plate counts. The HIB agar plates were incubated at 30°C for 48 h before enumerating bacteria (cfu/ml).

For flow cytometric/immunofluorescence analyses, WT *Y. pestis* CO92, its isogenic capsular negative (*caf1*$^{-}$) mutant, and *Y. pestis-luc* were grown and harvested as we previously described [19]. The harvested bacteria were fixed with 4% formaldehyde, stained with capsular (F1) antigen antibodies followed by goat anti-mouse secondary antibodies conjugated with Alexa Fluor 488. After washing, the bacterial cells were resuspended in 2% formaldehyde and approximately 30,000 cells were acquired on FACS Canto (BD Biosciences, San Diego, CA). The data were analyzed using FACS DIVA software (BD Biosciences) and FCS Expression Version 3 (De Novo Software). For a negative control, we also stained cells with isotype-matched irrelevant antibodies (instead of the F1-specific antibodies). For performing immunofluorescence microscopy, an aliquot of fixed bacterial cells (10 μl) was absorbed on a poly-L-lysine-coated glass slide, which was dried and

mounted with a coverslip. The slides were then examined by using a Nikon Ti microscope (Melville, NY). For immunofluorescence imaging, we used secondary antibodies that were conjugated with Alexa Fluor 594.

4.3 Animal infections

For animal mortality studies, female Swiss Webster mice (n=5; 6–8 weeks old) were infected intranasally with either 5 LD_{50} of WT *Y. pestis* CO92 or *Y. pestis-luc2* (1 LD_{50} of WT *Y. pestis* CO92 is approximately 500 cfu) in an animal biosafety level 3 (ABSL3) facility in the Galveston National Laboratory [14]. Animal survival was monitored for a period of 30 days.

4.4 IVIBB and bacterial determination

For IVIBB, a previously published protocol was followed [16]. Briefly, animals (n=9) were infected with 15 LD_{50} of *Y. pestis-luc2* by the intranasal route. After 24, 36, 48, 60, and 72 h post infection, all mice were subjected to *in vivo* imaging using an IVIS 200 bioluminescent and fluorescence whole-body imaging workstation (Caliper Corp. Alameda, CA) after lightly anesthetizing the animals under isofluorane. The bioluminescent scale is provided within the figures and it ranges from most intense (red) to least intense (violet) scaled based on radiance intensity. Simultaneously, animals (n=15) were infected with 15 LD_{50} of *Y. pestis-luc2* by the intranasal route. After 24, 48, and 72 h post infection, these animals (n=5) were humanely sacrificed, and various organs such as lungs, spleen, and liver as well as blood were harvested, homogenized when necessary, and subjected to plate counts by using sheep blood (5%) agar plates (Becton Dickinson, Sparks, MD).

We also treated a group of mice (n=5) with a protective dose of levofloxacin after infection with 15 LD_{50} of *Y. pestis-luc2*. Levofloxacin was administered via the i.p. route once daily 24 h post- pneumonic challenge at 10 mg/kg/day for 6 consecutive days as previously described [13, 14].

Quantitation of radiance by regions of interest (ROIs) was accomplished using Living Image software (Caliper Life Sciences, Alameda, CA). ROIs of the same shape and area were replicated across images measuring total flux (ρ/sec) to determine radiance. Data obtained were then plotted against cfu for various organs and analyzed by linear regression using Sigmaplot (Systat Software, San Jose, CA).

Acknowledgments

Studies conducted for this manuscript were supported by the NIH/NIAID AI064389 and N01 AI30065 grants (AKC). JAR was supported by the National Aeronautics and Space Administration (NASA) cooperative agreement NNX08B4A47A as well as AI64389. We thank Dr. A.G. Torres, UTMB, for providing pUTmini-Tn*5::lux*Km2 plasmid and Ms. K. Johnston for her initial help in imaging. We also thank Dr. S. Massey for his initial help with the software to determine total flux. We would also like to acknowledge UC7 grant which facilitated our research in the Galveston National Laboratory.

References

1. Greenfield RA, Drevets DA, Machado LJ, Voskuhl GW, Cornea P, Bronze MS. Bacterial pathogens as biological weapons and agents of bioterrorism. The Amer J Med Sci. 2002; 323:299–315.
2. Inglesby TV, Dennis DT, Henderson DA, Bartlett JG, Ascher MS, Eitzen E, et al. Plague as a biological weapon: medical and public health management. Working Group on Civilian Biodefense. JAMA. 2000; 283:2281–90. [PubMed: 10807389]
3. Evans RG, Crutcher JM, Shadel B, Clements B, Bronze MS. Terrorism from a public health perspective. The Amer J Med Sci. 2002; 323:291–8.

4. Galindo CL, Rosenzweig JA, Kirtley ML, Chopra AK. Pathogenesis of *Y. enterocolitica* and *Y. pseudotuberculosis* in Human Yersiniosis. J Pathog. 2011; 2011:182051. [PubMed: 22567322]

5. Cully JFJ, Williams ES. Interspecific comparisons of sylvatic plague in prairie dogs. J Mammalogy. 2001; 82:894–905.

6. Perry RD, Fetherston JD. *Yersinia pestis*--etiologic agent of plague. Clin Microbiol Rev. 1997; 10:35–66. [PubMed: 8993858]

7. Heymann DL. Emerging and re-emerging infectious diseases from plague and cholera to Ebola and AIDS: a potential for international spread that transcends the defenses of any single country. J Contig Crisis Manag. 2005; 13:29–31.

8. Alvarez ML, Cardineau GA. Prevention of bubonic and pneumonic plague using plant-derived vaccines. Biotechnol Adv. 2010; 28:184–96. [PubMed: 19931370]

9. Alibek, K.; Handelman, S. The chilling true story of the largest covert biological weapons program in the world - told from inside by the man who ran it. Lederberg, J., editor. Biohazard: Random House Inc; 1999. p. 336

10. Ligon BL. Plague: a review of its history and potential as a biological weapon. Seminars in pediatric infectious diseases. 2006; 17:161–70. [PubMed: 16934711]

11. Galimand M, Guiyoule A, Gerbaud G, Rasoamanana B, Chanteau S, Carniel E, et al. Multidrug resistance in *Yersinia pestis* mediated by a transferable plasmid. The New Engl J Med. 1997; 337:677–80.

12. Guiyoule A, Gerbaud G, Buchrieser C, Galimand M, Rahalison L, Chanteau S, et al. Transferable plasmid-mediated resistance to streptomycin in a clinical isolate of *Yersinia pestis*. Emerg Infect Dis. 2001; 7:43–8. [PubMed: 11266293]

13. Peterson JW, Moen ST, Healy D, Pawlik JE, Taormina J, Hardcastle J, et al. Protection Afforded by Fluoroquinolones in Animal Models of Respiratory Infections with *Bacillus anthracis*, *Yersinia pestis*, and *Francisella tularensis*. Open Microbiol J. 2010; 4:34–46. [PubMed: 21127743]

14. Rosenzweig JA, Brackman SM, Kirtley ML, Sha J, Erova TE, Yeager LA, et al. Cethromycin-mediated protection against the plague pathogen *Yersinia pestis* in a rat model of infection and comparison with levofloxacin. Antimicrobial agents and chemotherapy. 2011; 55:5034–42. [PubMed: 21859946]

15. Rosenzweig JA, Jejelowo O, Sha J, Erova TE, Brackman SM, Kirtley ML, et al. Progress on plague vaccine development. Appl Microbiol Biotechnol. 2011; 91:265–86. [PubMed: 21670978]

16. Massey S, Johnston K, Mott TM, Judy BM, Kvitko BH, Schweizer HP, et al. In vivo Bioluminescence Imaging of *Burkholderia mallei* Respiratory Infection and Treatment in the Mouse Model. Front Mcrobiol. 2011; 2:174.

17. Nham T, Filali S, Danne C, Derbise A, Carniel E. Imaging of bubonic plague dynamics by in vivo tracking of bioluminescent *Yersinia pestis*. PloS one. 2012; 7:e34714. [PubMed: 22496846]

18. Black PN. The fadL gene product of Escherichia coli is an outer membrane protein required for uptake of long-chain fatty acids and involved in sensitivity to bacteriophage T2. J Bacteriol. 1988; 170:2850–4. [PubMed: 3286621]

19. Sha J, Endsley JJ, Kirtley ML, Foltz SM, Huante MB, Erova TE, et al. Characterization of an F1 deletion mutant of *Yersinia pestis* CO92, pathogenic role of F1 antigen in bubonic and pneumonic plague, and evaluation of sensitivity and specificity of F1 antigen capture-based dipsticks. J Clin Microbiol. 2011; 49:1708–15. [PubMed: 21367990]

20. Rosenzweig JA, Weltman G, Plano GV, Schesser K. Modulation of yersinia type three secretion system by the S1 domain of polynucleotide phosphorylase. J biol Chem. 2005; 280:156–63. [PubMed: 15509583]

21. Layton RC, Mega W, McDonald JD, Brasel TL, Barr EB, Gigliotti AP, et al. Levofloxacin cures experimental pneumonic plague in African green monkeys. PLoS Negl Trop Dis. 2011; 5:e959. [PubMed: 21347450]

22. Agar SL, Sha J, Foltz SM, Erova TE, Walberg KG, Baze WB, et al. Characterization of the rat pneumonic plague model: infection kinetics following aerosolization of *Yersinia pestis* CO92. Microb Infect/ Institut Pasteur. 2009; 11:205–14.

23. Agar SL, Sha J, Foltz SM, Erova TE, Walberg KG, Parham TE, et al. Characterization of a mouse model of plague after aerosolization of *Yersinia pestis* CO92. Microbiology. 2008; 154:1939–48. [PubMed: 18599822]
24. Hinnebusch BJ, Rudolph AE, Cherepanov P, Dixon JE, Schwan TG, Forsberg A. Role of Yersinia murine toxin in survival of *Yersinia pestis* in the midgut of the flea vector. Science. 2002; 296:733–5. [PubMed: 11976454]
25. Hinnebusch J, Cherepanov P, Du Y, Rudolph A, Dixon JD, Schwan T, et al. Murine toxin of *Yersinia pestis* shows phospholipase D activity but is not required for virulence in mice. Inter J Med Microbiol. 2000; 290:483–7.
26. Contag CH, Contag PR, Mullins JI, Spilman SD, Stevenson DK, Benaron DA. Photonic detection of bacterial pathogens in living hosts. Mol Microbiol. 1995; 18:593–603. [PubMed: 8817482]
27. Foucault ML, Thomas L, Goussard S, Branchini BR, Grillot-Courvalin C. In vivo bioluminescence imaging for the study of intestinal colonization by *Escherichia coli* in mice. Appl Environ Mcrobiol. 2010; 76:264–74.
28. Andreu N, Zelmer A, Fletcher T, Elkington PT, Ward TH, Ripoll J, et al. Optimisation of bioluminescent reporters for use with mycobacteria. PloS one. 2010; 5:e10777. [PubMed: 20520722]
29. Winson MK, Swift S, Hill PJ, Sims CM, Griesmayr G, Bycroft BW, et al. Engineering the luxCDABE genes from Photorhabdus luminescens to provide a bioluminescent reporter for constitutive and promoter probe plasmids and mini-Tn5 constructs. FEMS Microbiol Lett. 1998; 163:193–202. [PubMed: 9673022]
30. Meighen EA. Molecular biology of bacterial bioluminescence. Microbiol Rev. 1991; 55:123–42. [PubMed: 2030669]
31. Hensel M, Shea JE, Gleeson C, Jones MD, Dalton E, Holden DW. Simultaneous identification of bacterial virulence genes by negative selection. Science. 1995; 269:400–3. [PubMed: 7618105]

Highlights

- A bioluminescent *Y. pestis* strain expressing luciferase (*luc*) gene was generated.
- *Y. pestis-luc2* strain exhibited similar virulence in mice as the parental strain.
- By 48 h post infection, bioluminescence can be seen in mouse organs by imaging.
- No bioluminescence was seen in animals given levofloxacin 24 h after infection.
- Strong correlation was noted between bioluminescence and colony forming units.

Fig. 1A

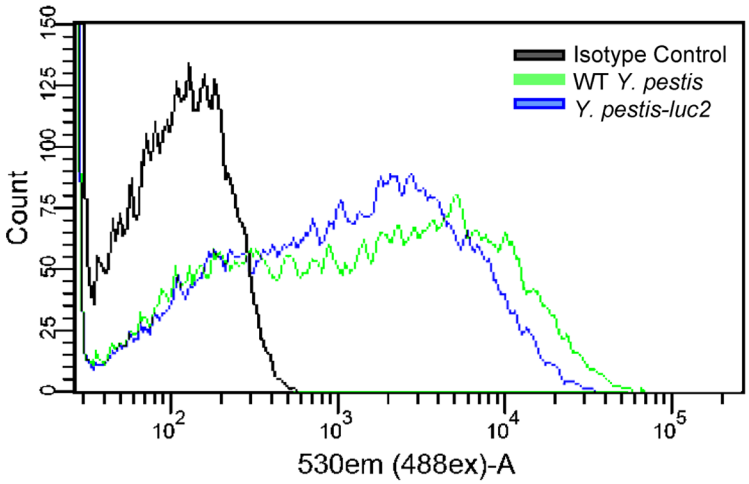

Fig. 1B

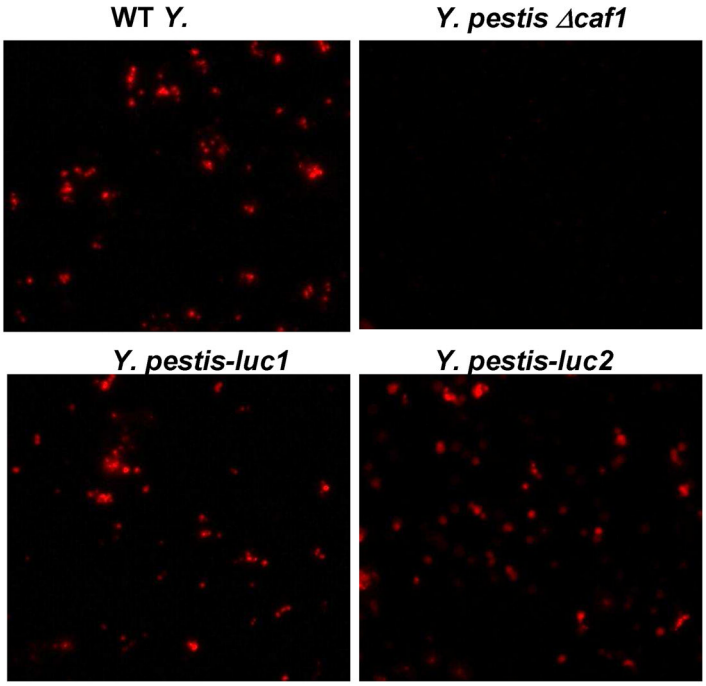

Figure 1.

A. Flow cytometric analysis of *Y. pestis-luc2* F1 antigen. The production of F1 antigen by the WT *Y. pestis* CO92 (green) and *Y. pestis-luc2* (blue) was evaluated by using specific antibodies to F1 or isotype-matched irrelevant antibodies (black), followed by detection with Alexa-488 labeled secondary antibodies. **B.** Immunofluorescence microscopy of fixed *Y. pestis* cells by using F1 primary antibodies and Alexa-594 conjugated secondary antibodies (magnification 400X).

Fig. 2A

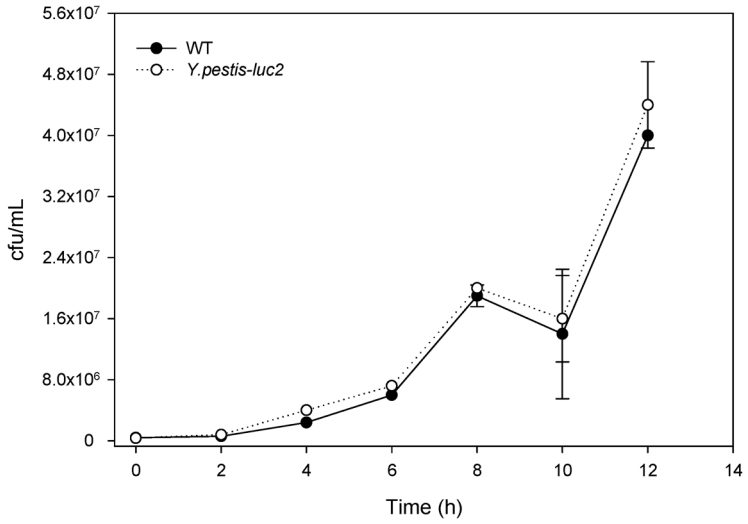

Fig. 2B

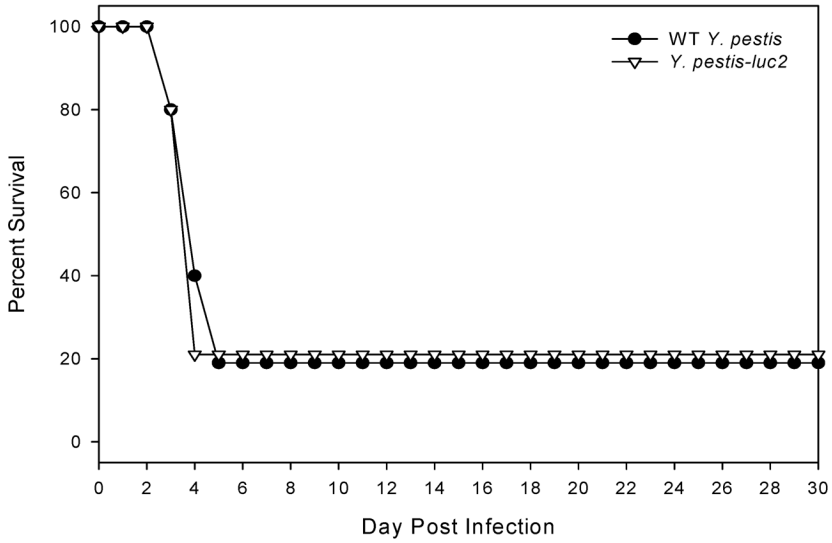

Figure 2.

Growth curve and 5 LD_{50} intranasal challenge of Swiss Webster mice (n=5). **A.** Growth curve data based on viable plate counts of both the WT and *Y. pestis-luc2* reporter strains is depicted. An arithmetic mean ± standard deviation was plotted from biological replicates. **B.** Percent survival of mice is graphically represented.

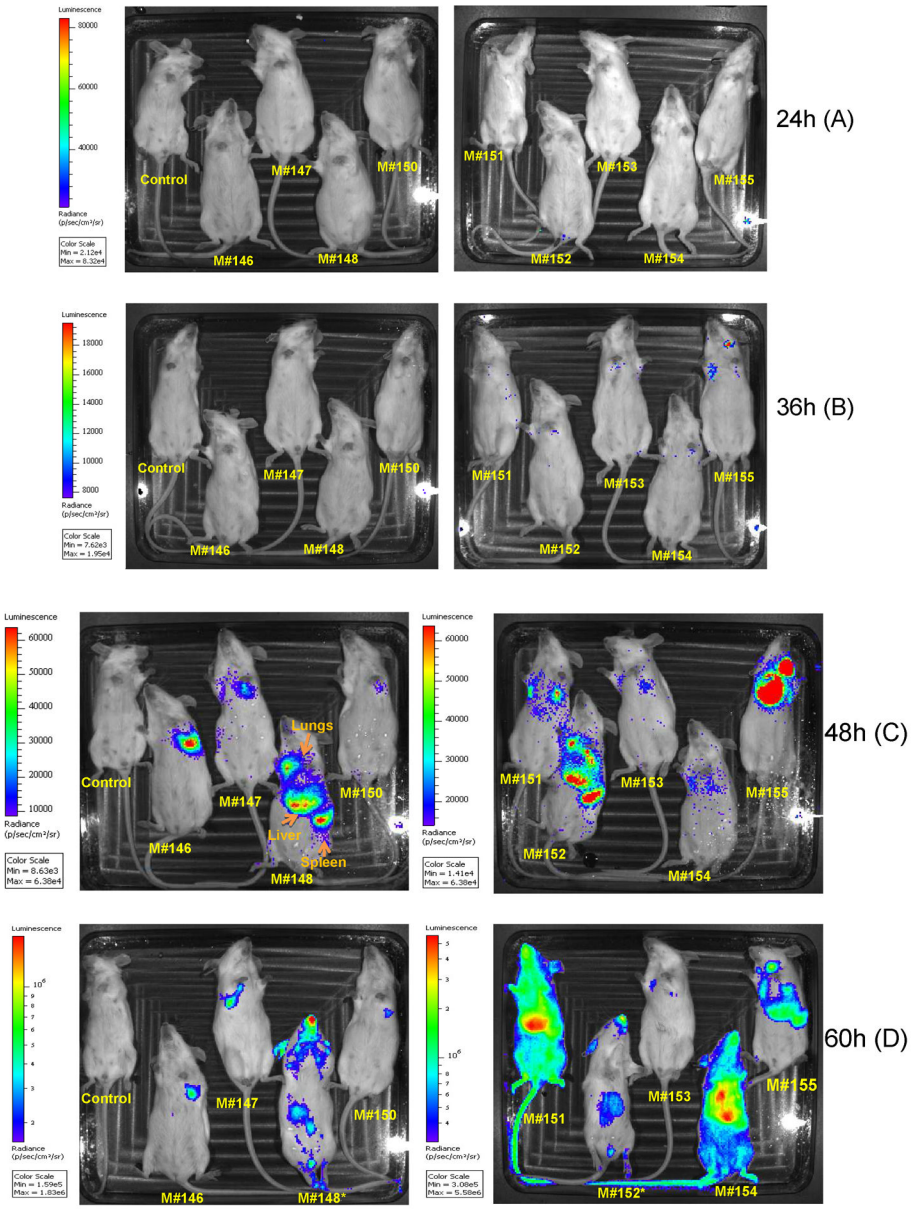

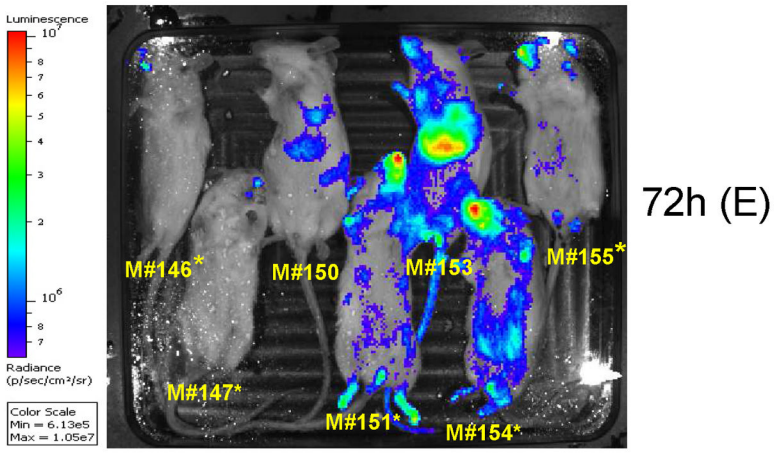

Fig. 3F

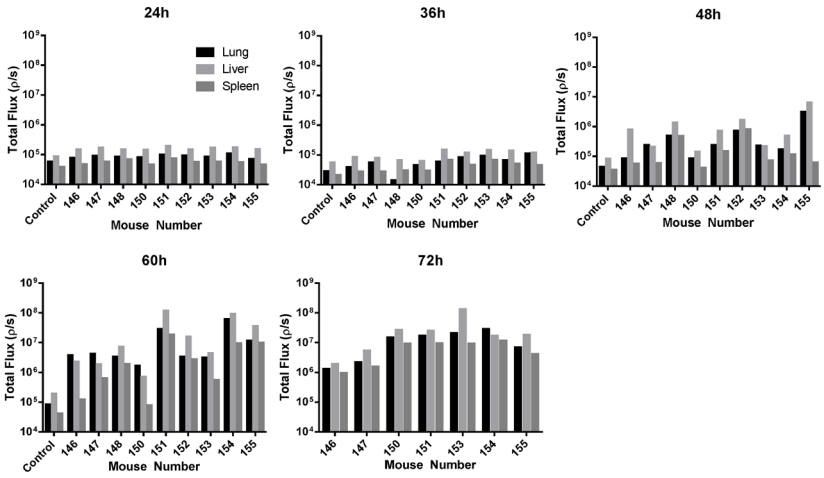

Figure 3.

Bioluminescence imaging of Swiss Webster mice. **A–E.** A group of 9 mice were intranasally challenged with 15 LD_{50} of *Y. pestis-luc2* and all animals were scanned at 24 **(A)**, 36 **(B)**, 48 **(C)**, 60 **(D)**, and 72 h **(E)** post infection. The bioluminescent scale is within the figures and ranges from most intense (red) to least intense (violet). Total flux was measured in ROIs, e.g., in lungs, and liver and spleen (time points 24–72 h) for all animals **(F)**. * represents those animals that were found dead but were imaged. Arrows point to ROIs (e.g., lungs, liver, and spleen).

Fig. 4A

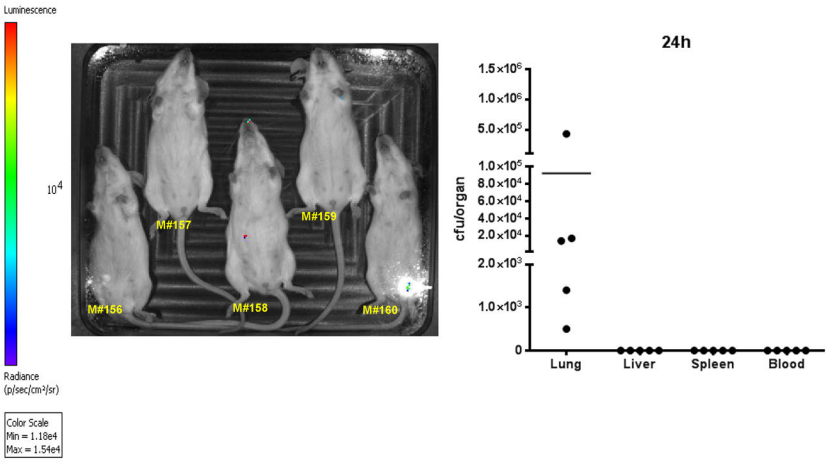

Fig. 4B

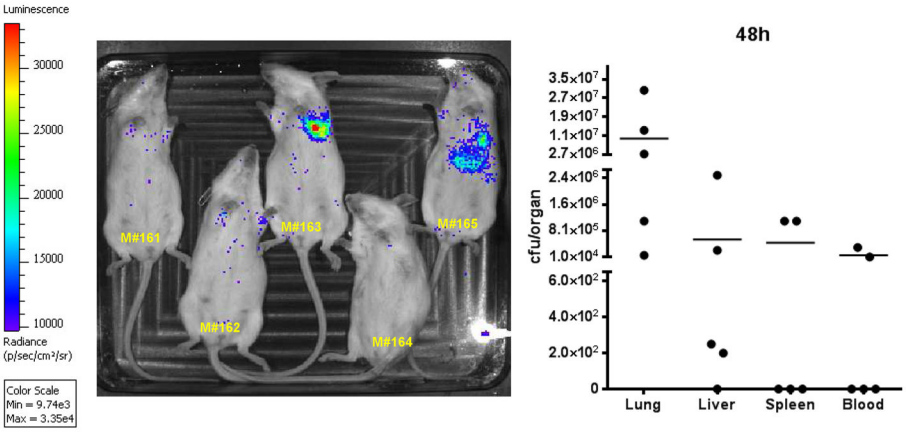

Fig. 4C

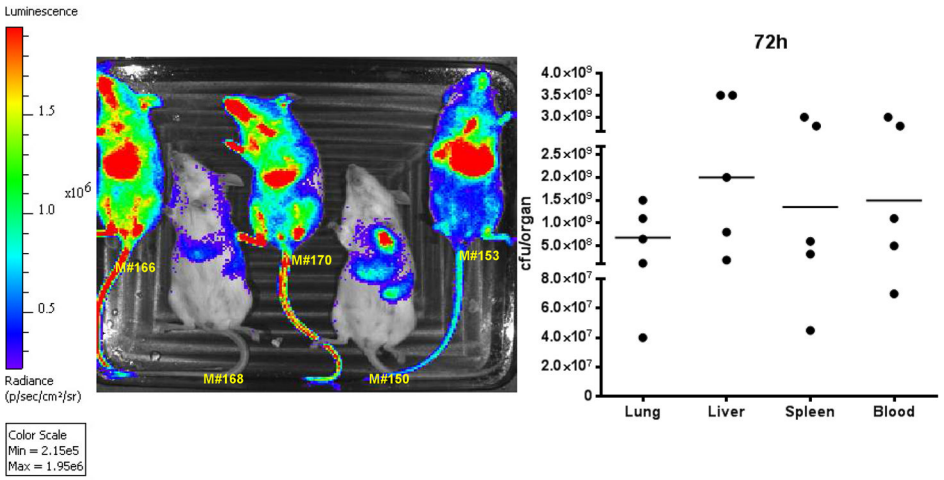

Fig. 4D

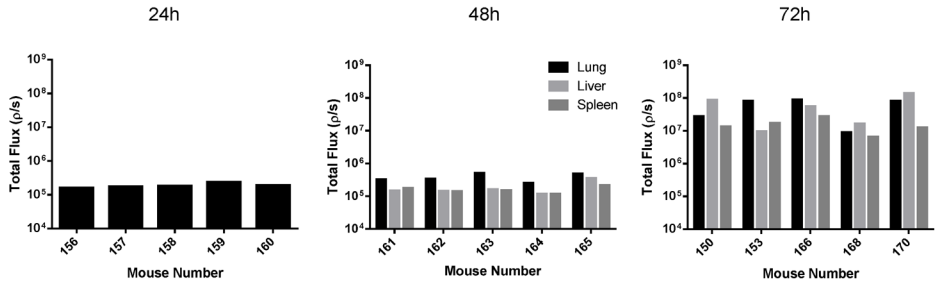

Fig. 4E

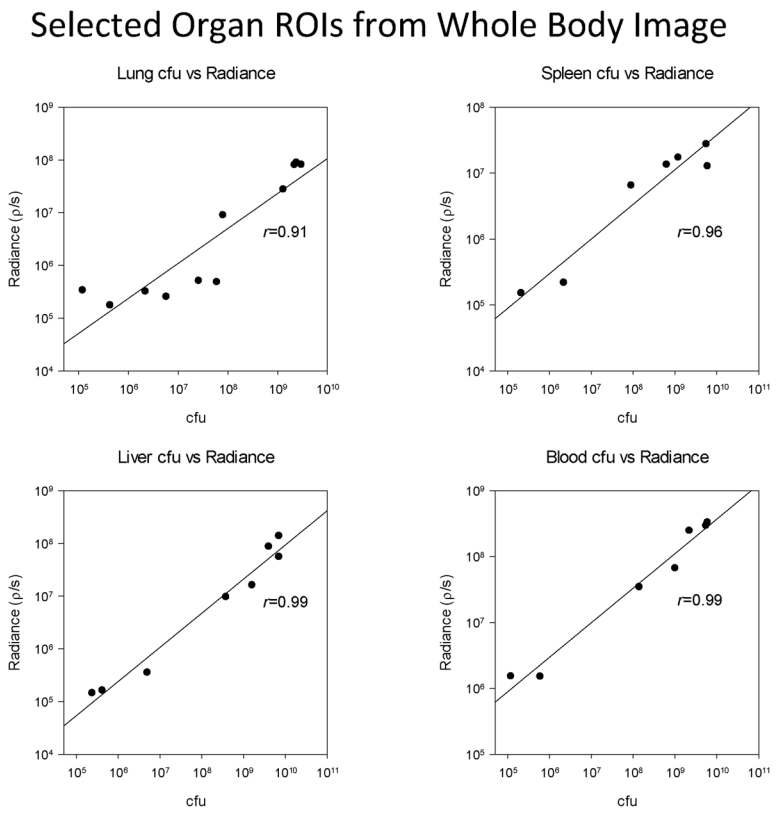

Figure 4.

Correlation between bioluminescent imaging (radiance) of whole mice and cfu loads (per organ or ml) in harvested tissues (lungs, liver, spleen, and blood) from Swiss Webster mice (n=15) 24 **(A),** 48 **(B)**, and 72 **(C)** h post-infection. The actual number of bacterial counts is also shown for all animals. The bioluminescent scale is within the figures and ranges from most intense (red) to least intense (violet). **D.** Total flux was measured in ROIs, e.g., in lungs (time points 24–72 h), and liver and spleen (time points 48–72 h) for all animals. **E.** Demonstrates correlation between radiance and cfu loads via linear regression of 24, 48, and 72 h samples, and R values are shown. Each point represents one animal. Points with cfu below 10^5 were excluded as they were outside the linear range of the data set.

Fig. 5A

24h

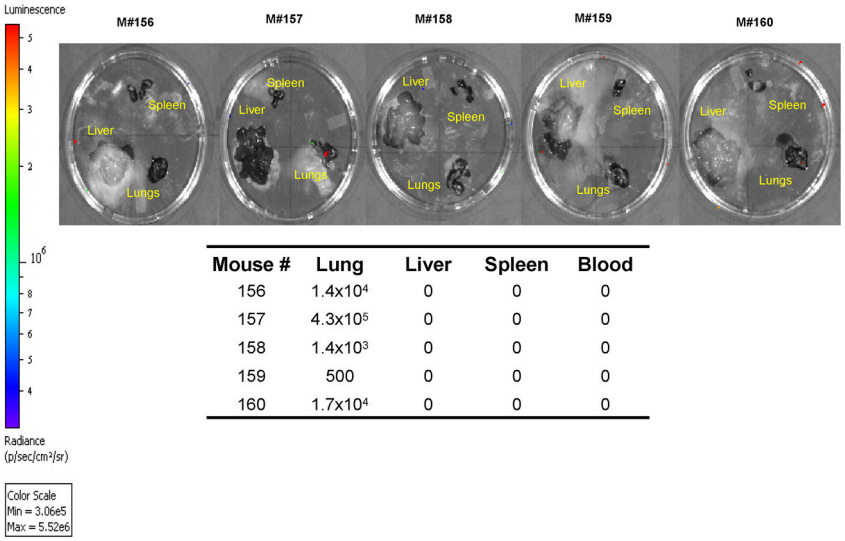

Mouse #	Lung	Liver	Spleen	Blood
156	$1.4x10^4$	0	0	0
157	$4.3x10^5$	0	0	0
158	$1.4x10^3$	0	0	0
159	500	0	0	0
160	$1.7x10^4$	0	0	0

Fig. 5B

48h

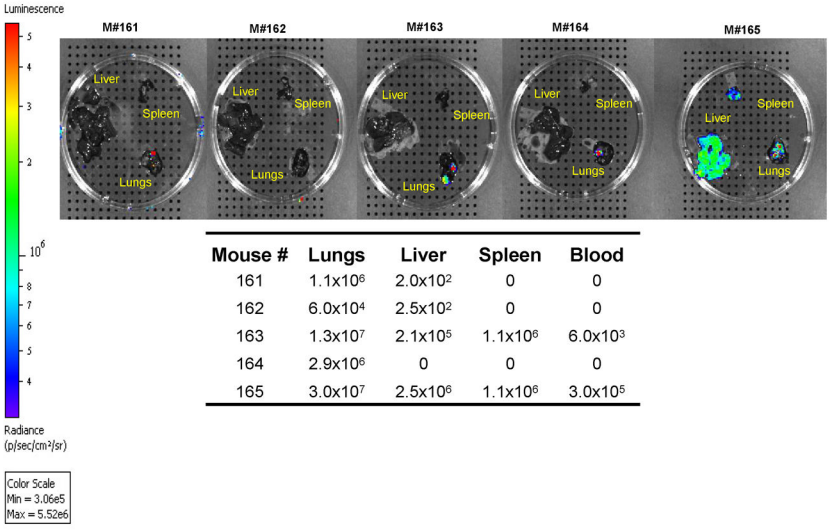

Mouse #	Lungs	Liver	Spleen	Blood
161	$1.1x10^6$	$2.0x10^2$	0	0
162	$6.0x10^4$	$2.5x10^2$	0	0
163	$1.3x10^7$	$2.1x10^5$	$1.1x10^6$	$6.0x10^3$
164	$2.9x10^6$	0	0	0
165	$3.0x10^7$	$2.5x10^6$	$1.1x10^6$	$3.0x10^5$

Fig. 5C

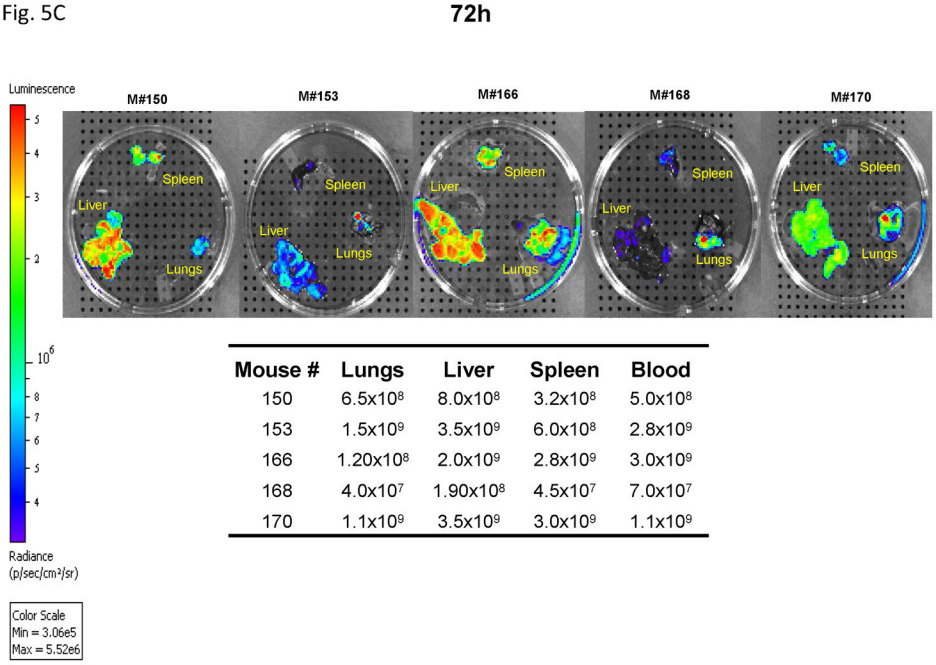

Mouse #	Lungs	Liver	Spleen	Blood
150	$6.5x10^8$	$8.0x10^8$	$3.2x10^8$	$5.0x10^8$
153	$1.5x10^9$	$3.5x10^9$	$6.0x10^8$	$2.8x10^9$
166	$1.20x10^8$	$2.0x10^9$	$2.8x10^9$	$3.0x10^9$
168	$4.0x10^7$	$1.90x10^8$	$4.5x10^7$	$7.0x10^7$
170	$1.1x10^9$	$3.5x10^9$	$3.0x10^9$	$1.1x10^9$

Fig. 5D

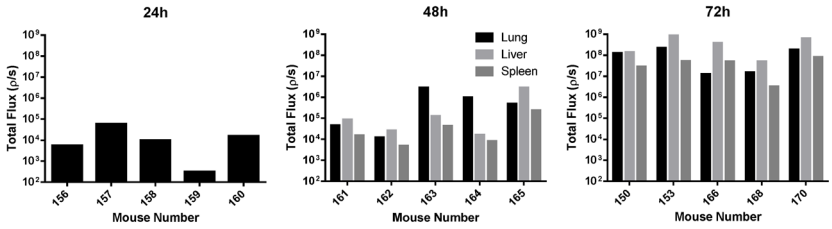

Fig. 5E

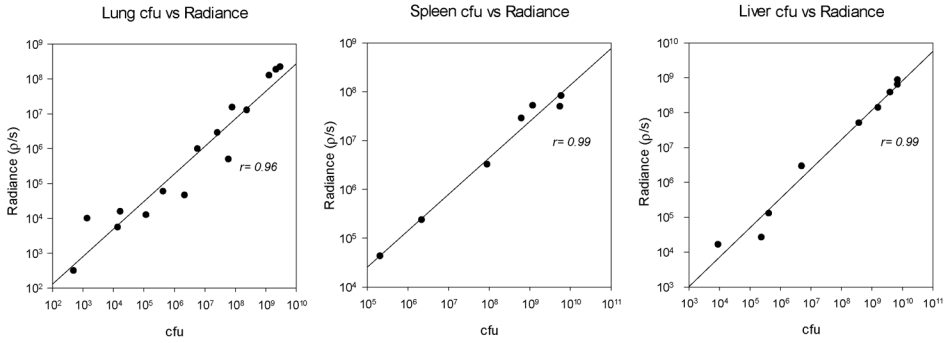

Figure 5.

Bioluminescent imaging and corresponding cfu loads of harvested lungs, spleen, and liver of *Y. pestis-luc2* infected mice (n=15) at 24 **(A)**, 48 **(B)**, and 72 **(C)** h post infection. The bioluminescent scale is within the figures and ranges from most intense (red) to least intense (violet). **D.** Total flux was measured in excised organs, e.g., in lungs (time points 24–72 h), and liver and spleen (time points 48–72 h) for all animals. **E.** Demonstrates correlation between radiance and cfu loads via linear regression of 24, 48, and 72 h samples, and R values are shown. Each point represents one animal. Points with cfu of zero were excluded.

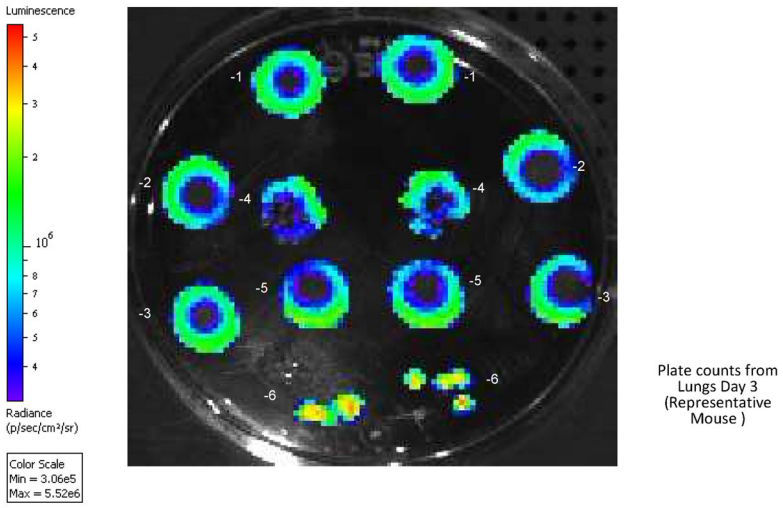

Figure 6.

Bioluminescent imaging of bacterial colonies derived from infected lung tissue 72 h post-infection of mouse #150 (Figure 5C). Cultures derived from infected lung tissue were diluted serially and plated in duplicate. The numbers 10^{-1} to 10^{-6} represent 10 fold dilutions. The bioluminescent scale is within the figures and ranges from most intense (red) to least intense (violet).

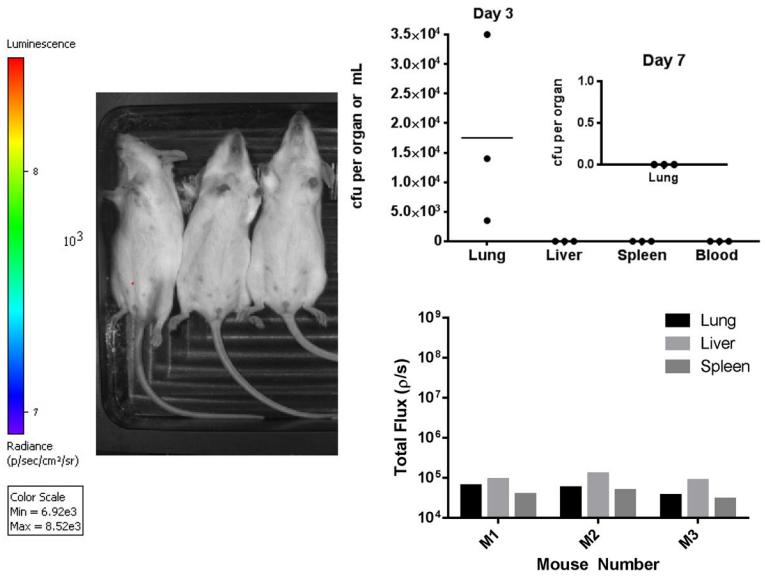

Figure 7.

Bioluminescent imaging 72 h post infection of Swiss Webster mice (n=5) treated with levofloxacin at 24 h post infection for 6 days. These animals were intranasally challenged with 15 LD_{50} of *Y. pestis-luc2* and were scanned for bioluminescence. Levofloxacin was administered to mice by the i.p. route at 10 mg/kg/day. Dissemination was monitored at 72 h post-infection by harvesting lungs, liver, spleen, and blood. Radiance was monitored using ROIs of mice at 72 h post-infection and represented as total flux in lungs, liver, and spleen of each animal. The bioluminescent scale is within the figures and ranges from most intense (red) to least intense (violet). The inset represents cfu in lungs from 2 remaining mice after 7 days of infection. The horizontal bar represents average number of bacteria per organ or ml of the blood.

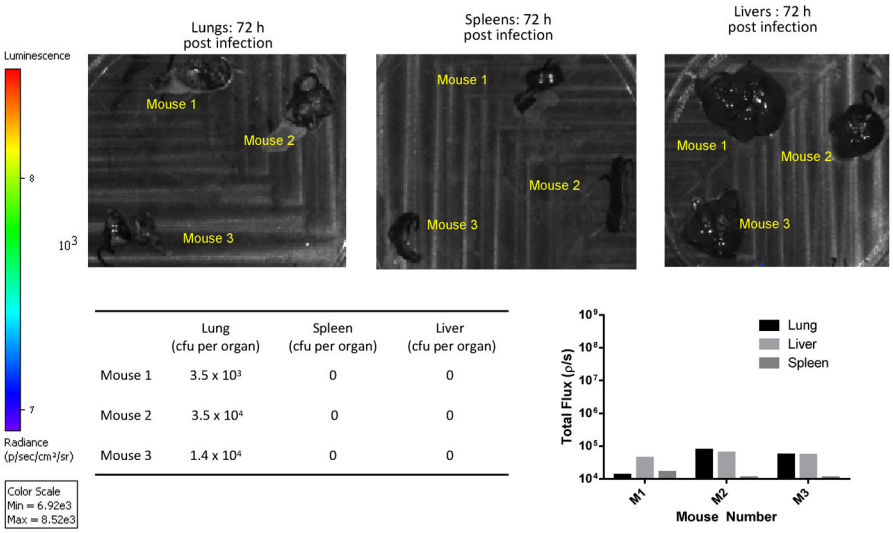

Figure 8.

Bioluminescent imaging of harvested tissues from 3 levofloxacin treated Swiss Webster mice 72 h post-infection (from Figure 7). Radiance was monitored in excised organs of mice at 72 h post-infection and represented as total flux in lungs, liver, and spleen of each animal. The tables show cfu in various tissues. The bioluminescent scale is within the figures and ranges from most intense (red) to least intense (violet).